NUMERICAL CALCULATION OF HEAT FLUX PROFILES IN A N_2O/C_2H_4 PREMIXED GREEN PROPELLANT COMBUSTOR USING AN INVERSE HEAT CONDUCTION METHOD

Nikolaos Perakis[(1)], Lukas Werling[(2)], Helmut Ciezki[(3)], Stefan Schlechtriem [(4)]

[(1)] Institute for Flight Propulsion, Technische Universität München (TUM), 85748 Garching, Germany, Email: nikolaos.perakis@tum.de

[(2)] Institute of Space Propulsion, German Aerospace Center (DLR), 74239 Hardthausen, Germany, Email: Lukas.Werling@dlr.de

[(3)] Institute of Space Propulsion, German Aerospace Center (DLR), 74239 Hardthausen, Germany, Email: Helmut.Ciezki@dlr.de

[(4)] Institute of Space Propulsion, German Aerospace Center (DLR), 74239 Hardthausen, Germany, Email: Stefan.Schlechtriem@dlr.de

KEYWORDS: Green propellants, nitrous oxide fuel blends, premixed monopropellant, N_2O, C_2H_4, inverse heat conduction, heat flux, wall temperature

ABSTRACT:

With the aim to replace toxic propellants like hydrazine, an effort has been placed in the investigation of human- and environment-friendlier substances called “Green Propellants”. Within the context of this research initiative and in terms with the REACH-Regulation, the German Aerospace Center (DLR) in Lampoldshausen is developing and testing an experimental demonstrator based on the technology of a premixed nitrous oxide/ethene (N_2O/C_2H_4) propellant. The advantages of this propellant include high specific impulse and low toxicity but are accompanied by several challenges like the high combustion temperature (up to 3300K), which directly influences the thermal design of an engine. For a better understanding of the combustion processes in the premixed propellant and a better estimation of the thermal loads on the thruster material, an accurate calculation of the heat flux in the combustion chamber is required. For this purpose an inverse heat conduction method developed at the Technical University of Munich (TUM) was utilized. Based on the thermocouple measurements in the chamber material, the time-dependant heat flux profiles were calculated using an Iterative Regularization Method (IRM). Heat flux and temperature results for different pressure load points were obtained, thereby helping to characterize the combustion properties of the propellant combination.

1. INTRODUCTION

A large fraction of current satellite propulsion systems used for station keeping, orbital and attitude control operate with hydrazine (N_2H_4). A big advantage of hydrazine is that can be used as a monopropellant with the use of a catalyst [1] or form a hyperbolic combination with a variety of oxidizers (like dinitrogen tetroxide) and combined with its good performance and relatively low cost has led to the establishment of this propellant as a common space propulsion fuel. Despite these benefits however, it poses a dangerous chemical substance due to its high toxicity and requires additional safety measures for the personnel handling it. For that reason, several initiatives to replace hydrazine from the space industry have been started, with the REACH-Regulation standing out within the European Union [2]. Within this regulation, the production and use of chemical substances are addressed, by taking into account the effects they impose on human health and the natural environment. Hydrazine is included among those substances, which directly translates to its potential future prohibition from the aerospace industry. In order to effectively substitute hydrazine, an increased amount of research resources has been invested by the aerospace community in finding alternative propulsion methods.

Aiming to reduce the environmental impact of rocket fuel and minimize the costs associated with health and safety precautions, low toxicity or green propellants stand in the focus of the scientific community. Promising candidates involve ionic liquids such as Ammonium Dinitramid (ADN) [3] or Hydroxylammonium nitrate (HAN) [4] based monopropellants, chlorine-free oxidants like hydrogen peroxide [5] and aluminum powder with water [6].

A further class of green propellants is the nitrous oxide fuel blends. These are composed of a mixture of hydrocarbons and nitrous oxide and serve as a “premixed monopropellant” system. The oxidizer (N_2O) and the fuel (e.g. C_2H_2, C_2H_4 or C_2H_6) are stored in a common tank, and are guided through a single feed line and a common injector into the combustion chamber, therefore

behaving as a monopropellant. The performance characteristics of the fuel are comparable to other bipropellant combinations (specific impulse close to 320 s) whereas their handling and injection is similar to classic monopropellants. Further advantages are the higher energy density compared to hydrazine [7] which allows for smaller tank volumes and the high vapor pressure of the components, which can lead to a self-pressurizing propulsion system. The most known nitrous oxide fuel blend is NOFBX patented by Firestar [8], [9].

Apart from the aforementioned benefits, nitrous oxide fuel blends require special design of the injection system to avoid flashback into the feed lines and potentially the tanks. Due to the premixed nature of the fuel, flame propagation upstream of the injector is possible and flashback arrestors are required to avoid it. Accidents that could be attributed to the flashback properties of the fuel, have been experienced by DARPA/Boeing's work on a nitrous oxide acetylene propellant mixture [10]. Furthermore the fuel demonstrates high combustion temperatures exceeding 3000 K, which directly relates to high thermal loads on the combustion chamber and nozzle walls. For that reason, active cooling is required and a detailed understanding of the combustion processes and heat release in the chamber is needed.

The German Aerospace Center (DLR) in Lampoldshausen is working on a nitrous oxide/ethene mixture [11-14] which was named "HyNOx" (Hydrocarbons mixed with Nitrous Oxide). As fuel ethene was chosen due to its similar vapor pressure compared to nitrous oxide (vapor pressure at 273K: C_2H_4: 41 bar; N_2O: 31.2 bar [7]). A result of the comparable vapor pressures is the good mixing characteristics leading to a homogenous mixture and the simultaneous evaporation in a propellant tank. Furthermore ethene is quite safe to handle, so compared to acetylene self-decomposition hazards can be avoided.

A demonstrator unit has been designed to operate with the premixed fuel and several tests on different load points have been carried out [15]. Since the rocket combustor has a capacitive cooling system and an upgrade to water active cooling is planned [12], the knowledge of the heat flux profiles on the hot gas chamber wall is important. The method presented in this paper provided with results of the hot gas wall temperature and the heat flux for different operational load points.

2. TEST SETUP AND COMBUSTOR DESIGN

The combustion tests were conducted at DLR's M11 test facility. A green propellant test container was assembled at the test bench M11.5 [11].

2.1. Test setup

To gain experience with the propellant mixture and to conduct the first tests, DLR chose to operate the mixture in its gaseous form. This way, the two components are stored in separate tanks and are mixed in gaseous state inside a common feeding line upstream the injector. The goal is to extend the test bench in order to accommodate a liquid mixture as well, but it was considered wiser to restrict the tests to gaseous form in the early development stages.

Using a gaseous mixture requires a less complex setup due to the lack of an evaporation facility. Moreover, different load points can be easily run by adjusting the feeding pressure and/or the orifice diameters in the feed lines, leading to a variation of the mixture ratio or the combustion pressure. Numerical investigations of the fuel's combustion process can also be compared more easily to the experimental data, since no phase change has to be modeled, thereby reducing the uncertainty of the results. A detailed description of the test facility can be found in [11], [15].

2.2. Combustor design

With regards to the combustion process and hence the heat release and heat flux profiles, the design of the rocket combustor is important. A section through the combustor can be seen in *Figure 1*.

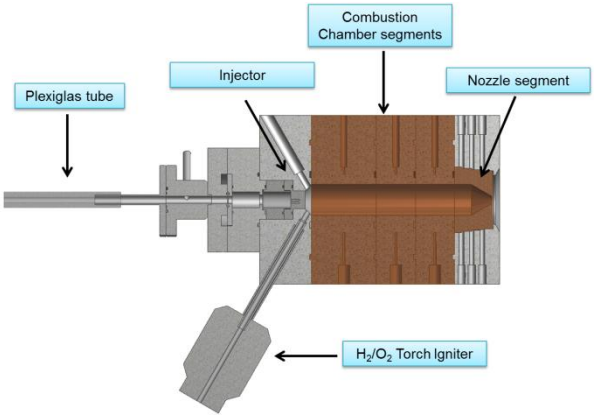

Figure 1: HyNOx Combustor

Within the feed line upstream the combustor, a Plexiglas tube is mounted. This is installed in order to optically examine a potential flashback of

the flame with a camera. Directly after the feed line, the propellants enter the injector. The tests described in the present paper were carried out with a showerhead injector consisting of 17 boreholes. Two of the originally foreseen boreholes were blocked by a drill during manufacturing, so only 17 of 19 injector holes were completely drilled. *Figure 2* shows a photo of the injector after manufacturing, where the blocked boreholes are visible. Each hole has a 0.65 mm diameter and a length of 4 mm. 12 of the holes are placed along a circle with 10 mm diameter, 6 of them are positioned along a circle with 5 mm diameter and a single hole is present in the middle of the injector.

Figure 2: Showerhead Injector

In order to ignite the mixture, a H_2/O_2 torch igniter was implemented as indicated in *Figure 1*. The igniter is equipped with hydrogen and oxygen feeding lines in which calibrated orifices are mounted. The orifices assure an oxygen/hydrogen mixture ratio of about 1.5 in case of a sonic flow. By using a big excess of hydrogen relatively low temperatures (1277K [16]) in the igniter were achieved. The overall igniter mass flow at the described tests was 1.3 g/s. The duration of the H_2/O_2 injection was limited to the first 1 s of the test run and after its shutdown, pure N_2O/C_2H_4 combustion was taking place in the chamber.

For the material of the HyNOx combustion chamber, the copper alloy elbrodur (CuCr1Zr) is used. The setup of the chamber allows for a modular design of the chamber's segments. As *Figure 1* illustrates, three chamber segments with different axial lengths were installed. In all the tests examined within this paper, the configuration's overall length is 110 mm; the first segment is 50 mm, whereas the other two are 30 mm long. The inner radius of the chamber measures 12 mm, whereas the outer one is 65 mm. For the diagnostics of the combustor operation, each segment is equipped with a pressure sensor and three thermocouples, which are located at the axial center of each segment. The pressure transducer measures the static pressure of the hot gas, whereas the three thermocouples measure the wall temperature at 3 mm, 8 mm and 12 mm radial distance from the inner combustion chamber wall.

The configuration of the sensors within the chamber segments is given in *Figure 3*.

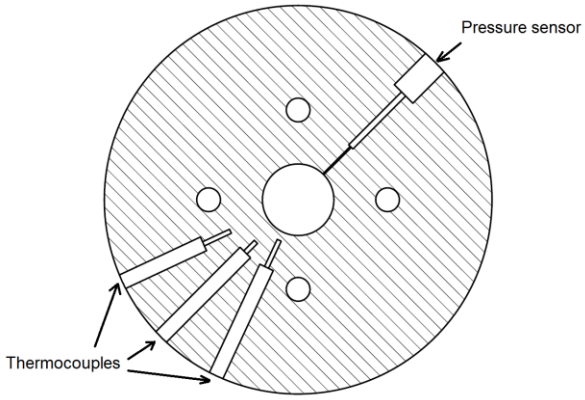

Figure 3: Pressure and temperature sensors in the combustion chamber segments

The thrust chamber is completed by a nozzle segment, which is again designed modularly, in order to allow for nozzles with different throat diameters and expansion ratios. During the described tests a truncated nozzle with a throat diameter of 5 mm was used. No sensors are installed within the nozzle segment and hence this is excluded from the present analysis, as explained in Section 3.2.

The temperature sensors were installed with the purpose of controlling the chamber wall temperature and providing information about the combustion process. With this information available, the calculation of the heat flux profile within the chamber was possible. In order to achieve that, an inverse heat conduction method was implemented as described in Section 3.

3. INVERSE HEAT CONDUCTION METHOD

The method utilized within the framework of this paper was developed at the Technical University of Munich [17], [18]. It is based on an Inverse Regularization Method (IRM) using a conjugate gradient optimization [19], [20] and was implemented with a 3D Finite Difference scheme in Matlab.

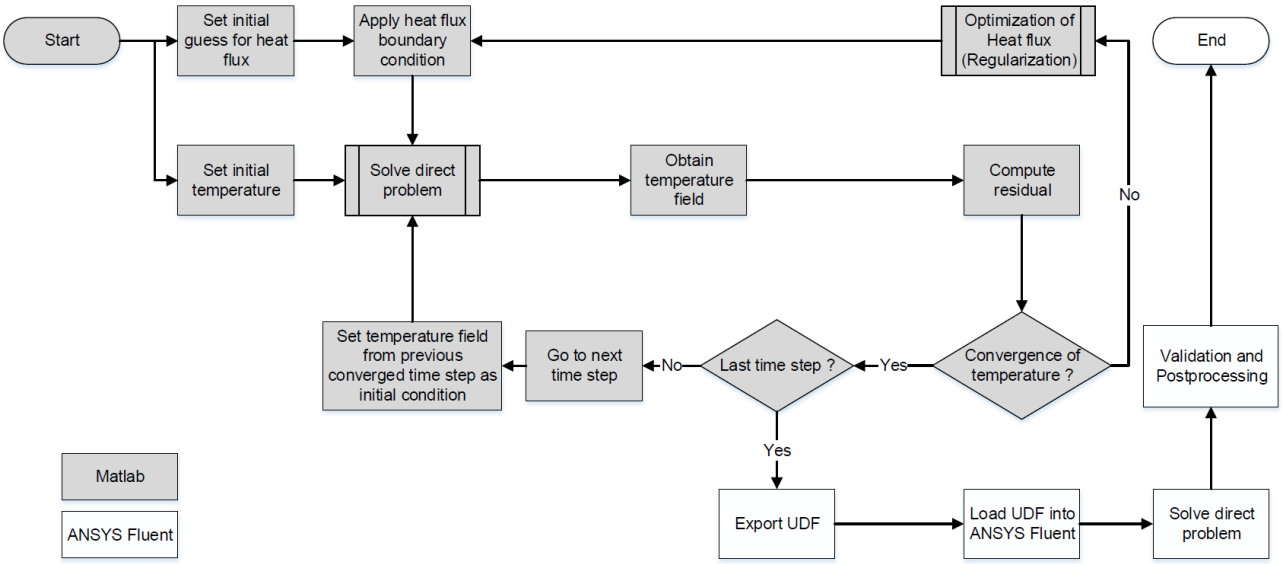

Figure 4: Flow chart of iterative solution of the inverse heat conduction problem

3.1. Theoretical background

In a classical direct heat transfer problem, the boundary conditions (heat flux) are known and applied to obtain a temperature field over space and time. In most engineering applications and especially in rocket engines, the temperature values at specific points within the combustion chamber or the nozzle are known when thermocouples are installed, whereas the thermal load (heat flux) on the hot gas walls is unknown. Using the provided temperature measurements to determine the heat flux leads to the formulation of an inverse problem, since the applied boundary condition is the unknown quantity. Inverse heat transfer problems are challenging due to their ill-posed nature as well as because surface conditions must be obtained from temperature sensors embedded within the objects, which experience attenuated and time-delayed responses to changes in boundary conditions.

The modeling approach of the inverse heat conduction examines only the thermal excitation of the material and does not simulate the fluid dynamical and thermodynamic processes in the hot gas. All these processes are modeled as a black box, whose only output is the heat flux, the variable sought for. The computational domain therefore consists only of the chamber material and the heat flux is defined as the boundary condition on the surfaces being in contact with the hot gas.

An iterative solution of this inverse problem includes the solution of the direct heat conduction multiple times, until convergence is achieved. A schematic overview of this process for the method applied in this paper is shown in *Figure 4*.

After the definition of the chamber's geometry and mesh, the initial temperature is set along the domain. For the initial temperature, the value at the thermocouple locations is used for t=0 s. It is important that the temperature field in the chamber at the beginning of the test does not demonstrate big fluctuations. The temperature is namely measured only at specific locations, but the code requires an initial temperature for all computational points and therefore performs an extrapolation of the measured values. If temperature differences higher than 10 K are present within the chamber material, which cannot be provided to the code, the initialization can induce errors into the predicted heat flux.

To begin the simulation, a value for the heat flux should be guessed and applied to the boundaries. A robust code should be able to converge independently of the initial solution, however a prediction of the heat flux close to the actual value, can lead to bigger stability and speed up the convergence.

With the initial and boundary conditions defined, the direct problem is solved. For this solution a finite difference scheme was programmed in Matlab. After solving the direct problem, the temperature field along the whole chamber is obtained. At this point a comparison between the computed and measured values of the temperature at the thermocouple locations takes place. Since the only information available is the temperature at the sensor positions, the solution is found when the calculated temperature matches the experimental one. A metric representing the difference between the two

values for the M installed thermocouples is the residual J, which is defined as in Equation (1):

$$J = \sum_{n=1}^{M} \int_{t}^{t+\Delta t} \left(T_C(\boldsymbol{x_n}, t) - T_M(\boldsymbol{x_n}, t)\right)^2 \mathrm{d}t \qquad (1)$$

Here T_C and T_M are the calculated and measured temperatures respectively, whereas $\boldsymbol{x_n}$ represents the location of each thermocouple and t the time. Note that $\boldsymbol{x_n}$ is a three dimensional vector and therefore a bold notation is used. J is also the cost function which has to be minimized during this inverse optimization problem. If the value of J is still quite large for the current time step, the optimization procedure is started. The optimization is carried out by utilizing the Lagrange functional L. This is a sum of the necessary conditions that have to be met in order for the problem to be well-defined. It is given by Equation (2):

$$L = \sum_{i=1}^{4} g_i \cdot f_i \qquad (2)$$

where f_i are the equality conditions and g_i the respective Lagrange multipliers. The equality conditions f_i are given by Equations (3) to (6):

$$f_1 = J \qquad (3)$$

$$f_2 = \int_0^t \oint_V \left(\nabla^2 T(\boldsymbol{x}, t) - \frac{1}{\alpha}\frac{\partial T(\boldsymbol{x}, t)}{\partial t}\right) \mathrm{d}V \mathrm{d}t \qquad (4)$$

$$f_3 = \oint_V \left(T_C(\boldsymbol{x}, t=0) - T_M(\boldsymbol{x}, t=0)\right) \mathrm{d}V \qquad (5)$$

$$f_4 = \int_0^t \oint_S \left(\dot{q}(\boldsymbol{x}, t) + \lambda \frac{\partial T(\boldsymbol{x}, t)}{\partial \boldsymbol{n}}\right) \mathrm{d}S \mathrm{d}t \qquad (6)$$

The second term f_2 is the Laplace heat conduction equation with α representing the heat diffusivity of the chamber material. f_3 stands for the initial condition at the computational domain (denoted by V) and finally f_4 represents a Neumann boundary condition at the surface S. In this condition, λ is the heat conductivity of the material, $\boldsymbol{n}$ the vector normal to the surface and $\dot{q}(\boldsymbol{x}, t)$ the unknown heat flux. With the Lagrange functional, the problem is modified from minimizing J, to minimizing L, i.e. to minimizing J while the constraints of the heat conduction law, the initial and boundary conditions are satisfied.
The optimality condition hence yields:

$$\delta L\left(\dot{q}(\boldsymbol{x}, t), \delta\dot{q}(\boldsymbol{x}, t)\right) = 0 \qquad (7)$$

In Equation (7) δL is the variation of the Lagrange functional and $\delta\dot{q}$ the variation of the heat flux. The minimization is carried out with a conjugate gradient method, which makes use of two parameters (the descent direction and the descent parameter) in order to update the solution of the unknown variable.
Equation (7) gives rise to two new set of partial differential equations: the direct variational problem and the adjoint problem [19]. The details of these two sets of equations can be found in [19], [18] and will not be further analyzed in this paper. Solving the two problems leads to an expression for the variation of the heat flux $\delta\dot{q}(\boldsymbol{x}, t)$, which is also the descent direction of the conjugate gradient method. Finally, the descent parameter γ is calculated from the results of the direct variational problem. This way, the updated solution for the heat flux in iteration step $\kappa + 1$ can be given by:

$$\dot{q}_{\kappa+1}(x, t) = \dot{q}_{\kappa} + \gamma \cdot \delta\dot{q}(x, t) \qquad (8)$$

The newly calculated heat flux is applied as a boundary condition and the calculated temperature field of the previous time step is used as an initial condition for the solution of the direct problem.
This process is repeated until the current time step converges, i.e. J drops below a predefined threshold. Then the calculation of the next time step begins. As soon as the final time step converges, the calculation is over and the results are exported. In order to validate the results and perform the postprocessing, an interface to the commercial solver ANSYS is established. The resulting heat flux from the inverse problem is used as a boundary condition in ANSYS' direct problem. When the direct solution is calculated, the temperature profiles between experimental data, inverse method results and direct solution results (ANSYS) are compared. For the application of the time dependent heat flux profiles into ANSYS, User Defined Functions (UDF) [21] are created in Matlab and are loaded into ANSYS.

3.2. Application of the inverse method on the HyNOx combustion chamber

The inverse heat conduction method was applied to the HyNOx combustion chamber and specifically, the thermocouples installed inside the copper material were utilized to provide the temperature information for the estimation of the heat flux. As seen in *Figure 1* and *Figure 3*, there are three axial positions along the chamber, with installed thermocouples and each axial position accommodates three sensors at different radial and azimuthal positions. The axial positions are located at 25 mm, 65 mm and 95 mm from the

faceplate. Due to the limited number of temperature sensors along the axis, no detailed axial resolution of the heat flux profile can be obtained. The main purpose of applying the method lies in calculating the value of the maximal occurring heat flux for different load points and hence understanding how the pressure and mass flow variation can influence the thermal load on the structure.
After the first calculations, it was established that the thermocouples located at 8 mm and 13 mm radial distance from the hot gas wall, demonstrated a very low sensitivity to the applied heat flux and hence the results were suffering from large uncertainties. To overcome this, a simplification was made and only the thermocouples at 3 mm were utilized in the simulation. This resulted also in a simplified geometry, since all the 3 mm sensors are located at the same azimuthal plane. The 3D domain could hence be transformed into an axisymmetric 2D domain with three measurement points along the axial direction. The simplified computational domain is depicted in *Figure 5*.

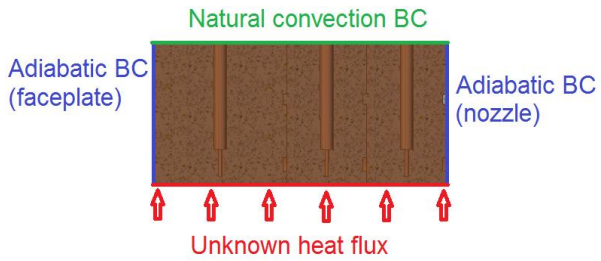

Figure 5: Applied boundary conditions (BC) in the computational domain

Since no temperature information is known in the nozzle segment, only the combustion chamber is included in the computational domain, with a total length of 110 mm. The faceplate and the nozzle are hence implemented only as adiabatic boundary conditions. The outside wall in contact to the environment is modeled as a natural convection boundary condition with a convective heat transfer coefficient $h = 15\,\mathrm{W/(m^2K)}$. The unknown heat flux was applied as the boundary condition at the hot gas wall. The material properties of the chamber material were considered to be constant and not temperature dependent.
Since the heat flux could only be calculated at the axial positions of the thermocouples, a linear interpolation was implemented for all other axial coordinates.

4. HEAT FLUX RESULTS

4.1. Scaling of heat flux with pressure

Four different load points from the same test campaign were examined and compared to each other as shown in *Table 1*. Each test load point consisted of two repetitions, and the average values are shown here. During all those tests the mixture ratio was close to the stoichiometric conditions (9.41) but underwent a variance of up to 1.3 among the different load points. All operating pressures in the chamber were kept low, with the highest one being slightly underneath 9 bar.

Table 1: Test load points

Test-No.	Average mass flow [g/s]	Mixture Ratio (O/F)	Average chamber pressure [bar]
HyNOx209	4.45	10.82	3.15
HyNOx210	6.76	10.3	4.89
HyNOx211	9.57	9.45	7.04
HyNOx212	12.06	10.09	8.83

In order to demonstrate the convergence of the code, a comparison between the measured and the calculated temperature values is shown for the case of the HyNOx212 test (8.83 bar) in *Figure 6*. The left subfigure demonstrates the measured temperature increase at the locations of the thermocouples, whereas the right subfigure illustrates the error between measured and calculated temperature $(\mathrm{T_M} - \mathrm{T_C})$. The numerical optimization error remains below 0.25 K, thereby proving the sufficient convergence of the inverse method.
The names of the thermocouples follow the convention T-BK-XX-YY, with XX standing for the axial position (one to three) and YY the radial distance from the hot gas wall in mm. It evident that the axial positions closer to the injector demonstrate a higher temperature than positions further downstream. This trend was observed in the experimental data of all four (4) load points and was also visible in the heat flux results as shown in the following paragraphs.

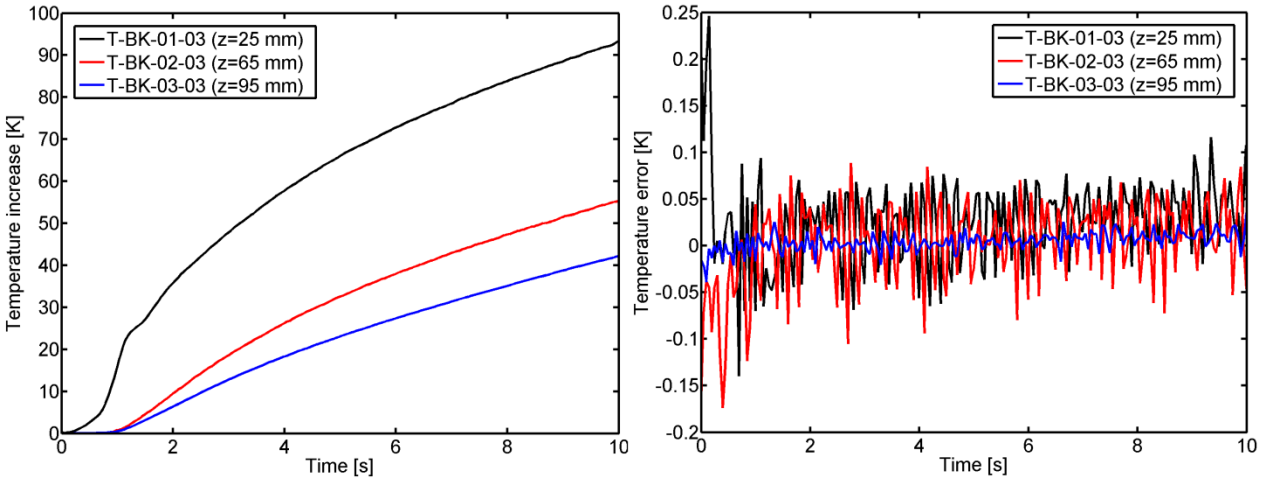

Figure 6: Temperature increase over time at the three thermocouple positions (left) and temperature error between measurement and calculation (right) for the 212 load point

This decrease of the wall temperature with the axial position implies that the flame front is anchored close to the injector and therefore the major fraction of heat release takes place close to the faceplate, whereas further downstream, the flow of the reaction products takes place. The decreasing wall temperature could indicate that no further reactions take place in the products (frozen flow) and that a cool-down of the products occurs due to heat exchange with the chamber wall.

Since the maximal temperature appears at locations close to the injector (thermocouple at the first axial position), the heat flux profiles examined in this section will involve the first axial position (z=25 mm) since it poses the most critical location along the chamber.

In order to get a more detailed insight into the heat flux profiles over time, the transient pressure data at the same location are shown in *Figure 7.* Directly after the opening of the valves, a sharp increase in the pressure is observed, which can be explained by the influence of the igniter. For the first 1 s, an excess mass flow of hydrogen and oxygen is present in the combustion chamber, which naturally increases the pressure above the nominal load point. After the operation of the igniter ceases, the pressure drops back into a constant value, which remains unaltered over time until the end of the test at t=10 s.

The corresponding heat flux results at the first thermocouple position are shown in *Figure 8*. As expected, a higher heat flux was observed with increasing chamber pressure. This is of course a result of the increased volumetric heat release of the mixture as well as of the higher mass flow rate which results in a more efficient heat exchange between the hot gas and the chamber walls. In order to quantify this increase, the heat flux after 10 s was examined as a function of the chamber pressure, with the related plot being illustrated in *Figure 9.* According to the applied fit of the numerical results, the relationship correlating the heat flux $\dot{q}$ and the pressure p is given by

$$\dot{q} \propto p^{0.68} \tag{7}$$

Heat transfer correlations available in literature such as Bartz [22] indicate that the heat transfer coefficient is proportional to the pressure to the power of 0.8. Of course, this scaling law is not universal and does not account for the different propellant combinations or different mixture ratios. It can however still capture the general dependence of the heat flux with increasing pressure and the present results validate that this dependence is almost linear at least for the low pressure regime examined during the HyNOx operation (3-9 bar).

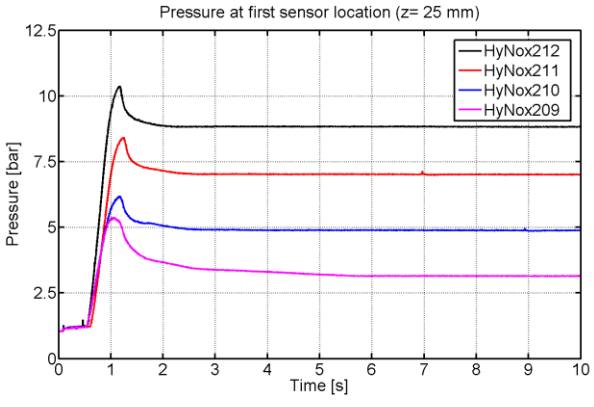

Figure 7: Pressure profile over time at z=25 mm

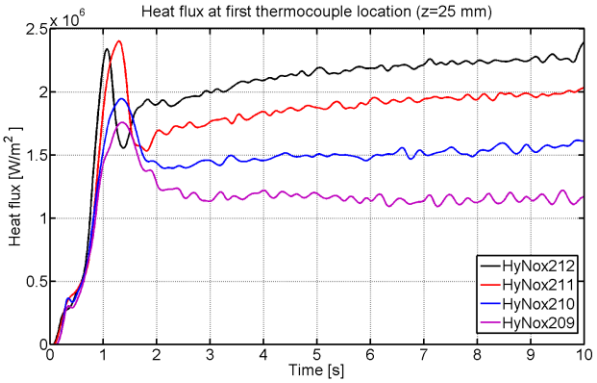

Figure 8: Heat flux profile over time at z=25 mm for different load points

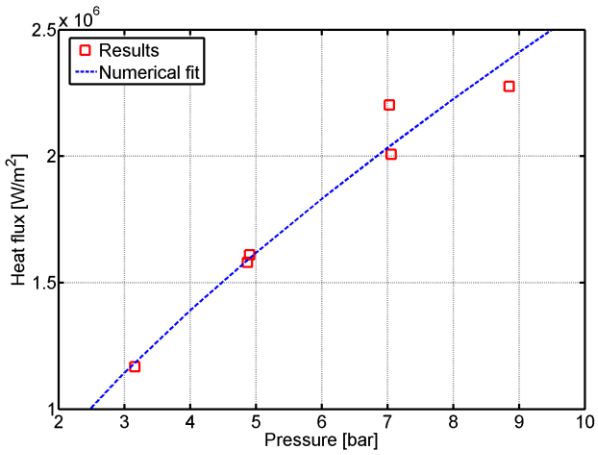

Figure 9: Correlation between chamber pressure and wall heat flux

Using the heat flux dependence on the pressure as a starting point, the scaling law of the calculated heat flux was compared with the theoretical heat release of an N_2O/C_2H_4 mixture. In order to obtain the theoretical heat release, the commercial chemistry tool Cantera was utilized [23]. Using the GRI3.0 reaction mechanism [24], the combustion of N_2O and C_2H_4 was calculated for equilibrium conditions under constant pressure and enthalpy (adiabatic, isobaric case). The total heat release for the reactions in the four load points of *Table 1* was calculated for the equilibrium conditions. The absolute and relative volumetric heat release rates for the four pressure points can be seen in *Table 2*. The relative heat released is normalized with the maximal value, i.e. the value corresponding to 8.83 bar.

It was expected, that a higher heat release rate would also imply a bigger heat flux on the walls, since a larger amount of energy is available in the chamber and can diffuse through conduction in the copper material. When comparing the theoretical results to the calculated heat fluxes as done in *Figure 10*, one observes that the theoretical heat release in equilibrium rises much faster with increasing pressure, compared to the wall heat flux. In fact it scales with the pressure to a power of approximately 2.90 compared to the 0.68 of the heat flux.

Table 2: Volumetric heat release for equilibrium N_2O/C_2H_4 combustion

Pressure [bar]	Volumetric heat release [W/m^3]	Relative volumetric heat release [%]
3.15	122	5.11
4.89	422	34.22
7.04	1232	51.63
8.83	2386	100.00

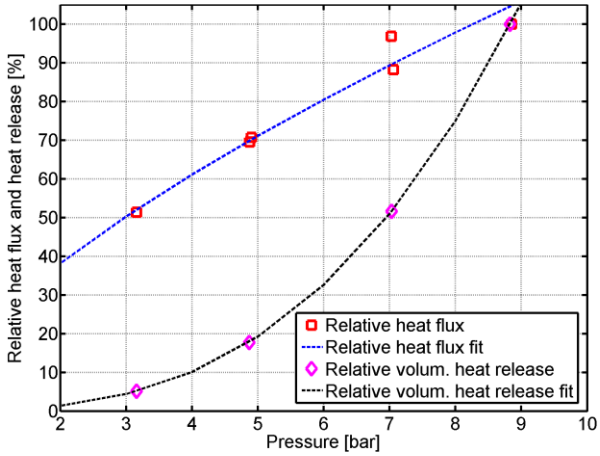

Figure 10: Comparison calculated heat flux and theoretical heat release

This discrepancy in the scaling of the heat flux and the heat release of the premixed monopropellant, gives useful information about the combustion process. The first piece of information that can be deduced is that the thermodynamic state of the gas within the combustion chamber is far from being in equilibrium. If the reactions were close to the chemical equilibrium, then one would expect that the heat flux would scale proportionally to the total heat being released in the chamber. The departure from equilibrium is expected for this propellant combination, especially for the low pressure regime. The complex reaction mechanism of the nitrous oxide combustion with ethene involves several slow reactions which lead to a large Damköhler number, when compared to faster chemical schemes like the H_2/O_2

combustion. Especially since the HyNOx combustion is highly turbulent, non-equilibrium effects are dominant in the chamber. Therefore, this fact could eventually be used when carrying out the future numerical simulation of the combustion process with CFD. One should expect that an equilibrium modeling of the N_2O/C_2H_4 chemistry would be insufficient to capture the process realistically and other methods like flamelet modeling and finite rate kinetics should be preferred.

A second explanation that could satisfy the results in *Figure 10* is that for higher pressures, the amount of heat diffusing outside the combustion chamber is reduced. This would imply that a smaller fraction of the heat released in the chemical reactions escapes the chamber and hence a larger fraction remains and can be utilized to accelerate the products and produce thrust. If this scenario was true, then one would expect the combustion efficiency to increase for larger pressures. This was actually observed in the HyNOx test campaign and the detailed results are presented at a separate paper by Werling et al. [15].

4.2. Transient profile of heat flux

Apart from the average heat flux over time at different load points, an examination of the transient profile can also give useful insight on the combustion processes in the HyNOx chamber. It is evident when comparing *Figure 7* and *Figure 8*, that the pressure increase caused by the igniter, also has a significant influence on the heat flux profile. Specifically, shortly after the beginning of combustion, the heat flux presents a peak before dropping again to its nominal value. This effect is present in all four (4) load points examined here. Another interesting effect of the igniter effect is that the aforementioned peak in heat flux occurs only for axial locations close to the injector. This can be visualized in *Figure 11*. In this figure, the results of the HyNOx209 test are presented, with the heat flux profile at the three thermocouple positions being plotted. The positions further downstream seem to be unaffected by the presence of the additional H_2/O_2 flow. This implies that the reaction zone of the igniter mass flow is restricted close to the injector, which is understandable considering the fast reaction rates of this propellant combination.

After the igniter is turned off, the heat flux should theoretically attain a constant plateau for the remaining duration of the test, assuming that the combustion is stable. As *Figure 8* shows, a qualitatively different behavior of the heat flux over time occurs for different pressure levels. Specifically, although the tests with low pressure (HyNOx209) demonstrate the expected constant heat flux over time, with higher pressure, an increase of heat flux over time is observed. Quantitatively, *Table 3* shows the relative increase of the heat flux value between t=3 s and t=10 s.

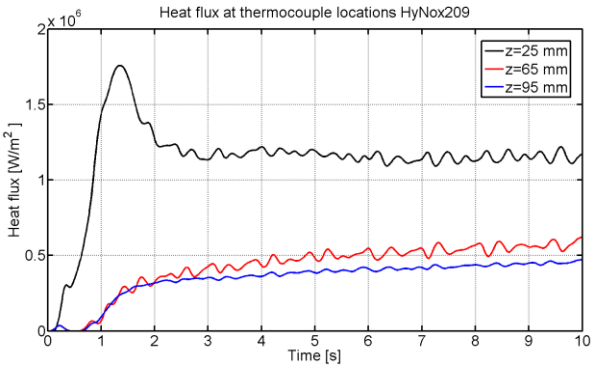

Figure 11: Transient heat flux profile for the HyNOx209 test

Table 3: Heat flux increase over time for different load points

Test Nr.	Heat flux t=3 s [MW/m^2]	Heat flux t=10 s [MW/m^2]	Relative heat flux increase [%]
209	1.14	1.14	0.00
210	1.45	1.57	8.28
211	1.77	2.01	13.56
212	2.00	2.29	14.50

A possible explanation for the transient phenomenon could be the effect of the copper wall temperature. During the experiment, the wall of the chamber gets heated up and hence poses a transient boundary condition. This effect, in combination to the catalytic effect that copper can have on the N_2O decomposition for high temperatures, could serve as a justification for the observed increase [25], [26]. With increasing test time, the copper temperature rises and so do the reaction rates of the surface reactions between the gas molecules, leading to a higher net heat release.

This assumption also explains why an increasing pressure leads to a faster heat flux increase over time as seen in *Table 3*. A higher pressure leads to a higher surface coverage θ, as the surface coverage is defined by Equation (8):

$$\theta = \frac{Kp}{1 + Kp} \tag{8}$$

K represents the equilibrium constant of the desorption reaction [27]. In the case of catalytic

N_2O decomposition, an oxygen radical is adsorbed by the catalytic wall and can lead to further oxidation of the ethene or other reaction products. A higher pressure should increase the number of adsorbed locations and hence also lead to a bigger heat flux increase over time. A detailed CFD simulation including surface reactions is planned in order to validate this assumption and explain the heat flux rise.

5. TEMPERATURE ON THE HOT GAS WALL

One of the main reasons why the knowledge of the heat flux is important in rocket engine applications is determining the temperature profile along the hot gas wall of the chamber and nozzle. Oxidation and phase change of the material is not desired and by better understanding the heat release mechanism of the propellant combination, a better estimation of the maximal wall temperature is possible.

With the heat flux data presented in Section 4, the temperature on the hot gas wall was calculated. In fact, since the solution of the inverse problem includes multiple solutions of the direct one, the temperature field is known along the whole combustion chamber. For the four (4) different load points, the axial temperature profile at the end of combustion (t=10 s) is plotted in *Figure 12*. As described in Section 4, the temperature seems to drop along the axis and therefore demonstrates its maximum close to the faceplate. One can also observe that close to the nozzle (110 mm), the temperature profile flattens out. This is a result of the adiabatic boundary condition applied on the chamber end and was chosen due to the lack of temperature information within the nozzle material. It would be interesting to examine the temperature profiles within the nozzle, especially close to the throat, which would require the installation of further temperature sensors.

For the HyNOx212 test case (~9 bar), the temperature profile along the chamber can be seen in *Figure 13*. This result was obtained with the commercial solver ANSYS Fluent, with the boundary conditions coming from the inverse method.

Since the HyNOx rocket combustor operates with a passive capacitive cooling system, the maximal duration of the test is limited by the temperature limits of the chamber material. With knowledge of the heat flux in various operational points, an estimation of the maximal test duration was carried out. The temperature limit was set at 400°C and the initial temperature of the chamber at 20°C. With this information, a maximal duration of 150 s was calculated for the 9 bar case. For lower pressures, longer durations are possible, as indicated by *Table 4*.

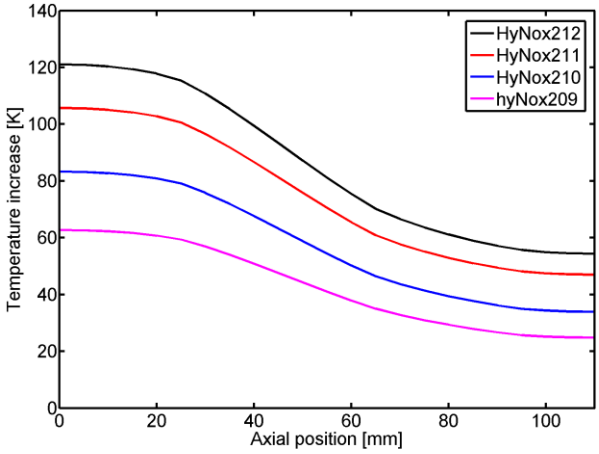

Figure 12: Temperature increase at the hot gas wall over axial position at t=10 s

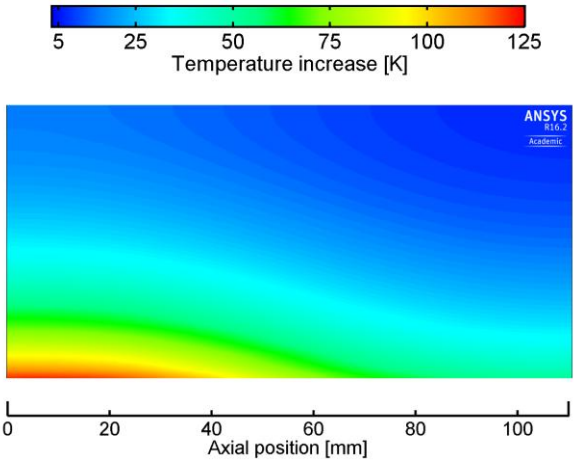

Figure 13: Temperature increase at t=10 s along the combustion chamber for HyNOx212

Table 4: Maximal test duration with capacitive cooling

Test Nr.	Maximal duration [s]
209	330
210	235
211	175
212	150

Longer test durations would be interesting in order to examine whether the heat flux increase vanishes after a specific time point and would therefore help understand the potential influence of the copper walls in more detail. For higher

pressures, than the ones presented in this paper, more caution is required and only shorter durations are allowed. However, steps have already been made in the direction of an active cooling system, which would enable a steady state operation and longer test durations [12].

6. OUTLOOK AND SUMMARY

The institute of Space Propulsion of the German Aerospace Center (DLR) has set up a test bench to examine the combustion and ignition of a N_2O/C_2H_4 premixed green propellant. With the first tests being available, an effort to characterize the heat release in the capacitive combustion chamber and the thermal load on the walls was made. A better knowledge of the heat flux leads to more accurate design of the cooling system and to a more detailed insight into the propellant combustion.

For that reason, an inverse heat conduction method was applied, taking as an input the temperature measurements of the thermocouples in the copper wall. With this information, the axial heat flux profile was calculated, indicating a declining heat flux value with increasing axial position. This feature was explained by a short length of the combustion zone and a flame anchored onto the injector.

As expected, a higher pressure load point leads to a higher heat flux value on the chamber walls. By understanding the dependence of the heat flux on the chamber pressure, an extrapolation can be made in order to predict the thermal load for other load points.

The transient profile of the heat flux results was also analyzed. The observation was made, that for low chamber pressures, the heat flux tends to reach a steady state value shortly after ignition. For higher pressures on the other hand, a constant increase of the heat flux was observed for the first 10 seconds of the test. This effect was attributed to the catalytic influence of the copper walls on the mixture's reactions and specifically the nitrous oxide decomposition. The increasing wall temperature serves as a transient boundary condition and for higher pressures, the surface reactions play a non-negligible role, leading to the transient rise of the heat flux.

Finally, using the calculated heat flux, the wall temperature in contact to the hot gas could be estimated. With this information, a better planning of the test durations can be made, in order to ensure that no thermal or mechanical damage of the chamber walls occurs during a test with capacitive cooling.

A continuation of the tests with gaseous propellants is planned for different load points and for higher pressures (>10 bar). Longer test durations are also scheduled, in order to examine whether the transient rise in heat flux remains over time or if it reaches a steady state. Furthermore, the installation of more thermocouples along the axis of the chamber will provide a higher axial resolution and hence a more complete heat flux profile, whereas sensors in the nozzle could help in the modeling of the boundary condition in the inverse method.

A thorough CFD simulation of the combustion process would be of interest in order to validate the assumption of the copper surface's catalytic effect and the axial drop of heat flux. The heat flux results presented in this paper will serve as a reference in order to verify the potential CFD results.

7. REFERENCES

[1] R. L. Sackheim, "Survay of Space Applications of Monopropellant Hydrazine Propulsion Systems," Combustion Systems Laboratory, TRW Systems Group (Redondo Beach, CA), 1973.

[2] ECHA, "Candidate List of substances of very high concern for Authorisation".

[3] K. Anflo and B. Crowe, "Two years of in-space demonstration and qualification of an ADN-based propulsion system on PRISMA," in 47th AIAA/ASME/SAE/ASEE Joint Propulsion Conference, San Diego, USA, 2011.

[4] R. A. Spores, R. K. Masse, S. Kimbrel and C. McLean, "GPIM AF-M315E Propulsion System," in 50th AIAA/ASME/SAE/ASEE Joint Propulsion Conference & Exhibit, Cleveland, Ohio, USA, 2014.

[5] U. Gotzig, S. Krauss, D. Welberg, D. Fiot, P. Michaud, C. Desaguier, S. Casu, B. Geiger and R. Kiemel, "Development and Test of a 3D printed Hydrogen Peroxide Flight Control Thruster," in 51st AIAA/SAE/ASEE Joint Propulsion Conference, Orlando, Florida, USA, 2015.

[6] T. Wood, M. A. Pfeil, T. L. Pourpoint and S. F. Son, "Aluminum-ice (ALICE) propellants for hydrogen generation and propulsion," in 45th AIAA/SAE/ASE Joint Propulsion Conference & Exhibit, 2009.

[7] E. W. Lemmon, M. L. Huber and M. O. McLinden, "NIST Standard Reference Database 23: Reference Fluid Thermodynamic and Transport Properties - REFPROP," National Institute of Standards and Technology, Gaithersburg, 2013.

[8] G. Mungas, M. Vozoff and B. Rishikof, "NOFBXTM: A new non-toxic, "Green" propulsion technology with high performance and low cost," in 63rd International Astronautical Congress, Naples, Italy, 2012.

[9] M. Gregory, D. J. Fisher, C. Mungas and B. Carryer, "Nitrous Oxide Fuel Blend Monopropellant". USA Patent US20090133788, 28 May 2009.

[10] "Spacenews.com," 31 March 2016. [Online]. Available: http://spacenews.com/darpa-airborne-launcher-effort-falters/.

[11] L. Werling, A. Gernoth and S. Schlechtriem, "Investigation of the Combustion and Ignition Process of a Nitrous Oxide/Ethene Fuel Blend," in Space Propulsion Conference, Cologne, Germany, 2014.

[12] L. Werling, B. Hochheimer, A. Baral, H. K. Ciezki and S. Schlechtriem, "Experimental and Numerical Analysis of the Heat Flux occurring in a Nitrous Oxide/Ethene Green Propellant Combustion Demonstrator," in 51st AIAA/SAE/ASEE Joint Propulsion Conference, Orlando, Florida, USA, 2015.

[13] L. Werling, N. Perakis, B. Hochheimer, H. K. Ciezki and S. Schlechtriem, "Experimental Investigations based on a Demonstrator Unit to analyze the Combustion Process of a Nitrous Oxide/Ethen Premixed Green Bipropellant," in 5th CEAS Air & Space Conference, Delft, Netherlands, 2015.

[14] N. Perakis, B. Hochheimer, L. Werling, A. Gernoth and S. Schlechtriem, "Development of an experimental demonstrator unit using Nitrous Oxide/Ethylene Premixed Bipropellant for satellite applications," in Meet the Space Conference, Krakow, Poland, 2014.

[15] L. Werling, N. Perakis, S. Müller, A. Hauk, H. K. Ciezki and S. Schlechtriem, "Hot Firing of a N2O/C2H4 Premixed Green propellant: First combustion tests and results," in Space Propulsion Conference, Rome, Italy, 2016.

[16] B. J. McBride and S. Gordon, "Computer Program for Calculation of Complex Chemical Equilibrium Compositions and Applications II," National Aeronautics and Space Administration, Lewis Research Center, Cleveland, Ohio, USA.

[17] M. P. Celano, S. Silvestri, N. Perakis, F. Schily and O. J. Haidn, "Heat Flux Evaluation Methods for a Single Element Heat Sink Chamber," in 6th European Conference of Aeronautics and Space Science, Krakow, Poland, 2015.

[18] N. Perakis, "Inverse Method applied to Rocket Combustion Chambers," Technische Universität München, Munich, Germany, 2014.

[19] E. Artioukhine, "Heat transfer and inverse analysis," RTO-EN-AVT-117, 2005.

[20] H. Cheng-Hung and C. Wei-Chung, "A three-dimensional inverse forced convection problem in estimating surface heat flux by conjugate gradient method," International Journal of Heat and Mass Transfer, vol. 43, pp. 3171-3181, 2000.

[21] A. Fluent, "Fluent 14.0 User's Guide," ANSYS FLUENT Inc, 2011.

[22] D. R. Bartz, "A simple equation for rapid estimation of rocket nozzle convective heat transfer coefficients," Journal of Jet Propulsion, 1957.

[23] D. G. Goodwin, H. K. Moffat and R. L. Speth, "Cantera: An Object-oriented Software Toolkit for Chemical Kinetics, Thermodynamics, and Transport Processes," 2016.

[24] G. P. Smith, D. M. Golden, M. Frenklach, N. W. Moriarty, B. Eiteneer, M. Goldenberg, T. C. Bowman, R. K. Hanson, S. Song, W. C. Gardiner, V. V. Lassianski and Z. Qin. [Online]. Available: http://www.me.berkeley.edu/gri_mech/.

[25] A. Satsuma, H. Maeshima, K. Watanabe, K. Suzuki and T. Hattori, "Effects of methane and oxygen on decomposition of nitrous oxide over metal oxide catalysts," Catalysis Today,

pp. 347-353, 2000.

[26] J. F. Scholten and J. A. Konvalinka, "Reaction of Nitrous Oxide with copper surfaces," Transactions of the Faraday Society, vol. 65, pp. 2565-2473, 1969.

[27] K. Christmann, "Thermodynamics and Kinetics of Adsorption," IMPRS-Lecture Series, 2012.

[28] I. A. Klepikov, B. I. Katorgin and V. K. Chvanov, "The new generation of rocket engines, operating by ecologically safe propellant “liquid oxygen and liquefied natural gas (methane)”," Acta Astronautica, vol. 41, no. 4, pp. 209-217, 1997.